Inorganic Chemistry

Article

pubs.acs.org/IC

The Influence of Heme Ruffling on Spin Densities in Ferricytochromes *c* Probed by Heme Core ^{13}C NMR

Jesse G. Kleingardner, Sarah E. J. Bowman, and Kara L. Bren*

Department of Chemistry, University of Rochester, Rochester, New York 14627-0216, United States

Supporting Information

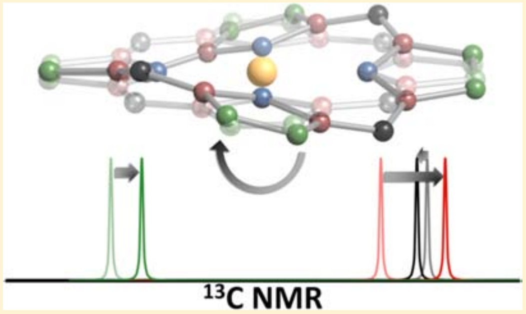

ABSTRACT: The heme in cytochromes *c* undergoes a conserved out-of-plane distortion known as ruffling. For cytochromes *c* from the bacteria *Hydrogenobacter thermophilus* and *Pseudomonas aeruginosa*, NMR and EPR spectra have been shown to be sensitive to the extent of heme ruffling and to provide insights into the effect of ruffling on the electronic structure. Through the use of mutants of each of these cytochromes that differ in the amount of heme ruffling, NMR characterization of the low-spin ($S = {}^{1}/_{2}$) ferric proteins has confirmed and refined the developing understanding of how ruffling influences the spin distribution on heme. The chemical shifts of the core heme carbons were obtained through site-specific labeling of the heme via biosynthetic incorporation of ^{13}C-labeled 5-aminolevulinic acid derivatives. Analysis of the contact shifts of these core heme carbons allowed Fermi contact spin densities to be estimated and changes upon ruffling to be evaluated. The results allow a deconvolution of the contributions to heme hyperfine shifts and a test of the influence of heme ruffling on the electronic structure and hyperfine shifts. The data indicate that as heme ruffling increases, the spin densities on the *β*-pyrrole carbons decrease while the spin densities on the *α*-pyrrole carbons and meso carbons increase. Furthermore, increased ruffling is associated with stronger bonding to the heme axial His ligand.

Structural characterization of heme proteins has demonstrated that hemes undergo nonplanar distortions[1] along low-frequency vibrational normal modes that are classified by the symmetry of the normal mode.[2] Saddling (B_{2u}), ruffling (B_{1u}), and doming (A_{2u}) are the most frequently observed nonplanar distortions in heme proteins, and the type of structural distortion typically is conserved among proteins that carry out the same function.[1,3] For example, saddling is conserved in peroxidases,[4] ruffling is seen in electron-transferring *c*-type cytochromes,[5,6] and doming is observed in oxygen storage and transport proteins such as myoglobin and hemoglobin.[3,7] The functional role of heme nonplanar distortions in proteins is not yet fully understood and has been the subject of recent discussion and research.[1,8]

Ruffling has been proposed to influence heme function in a number of proteins. In electron-transferring cytochromes *c* and in NO-carrying nitrophorins, ruffling has been shown to modulate the reduction potential.[5,9−11] Ruffling also has been suggested to lower the affinity for oxygen in nitric oxide/oxygen binding (H-NOX) proteins[11] and to influence the NO binding geometry in nitrophorins.[10,12] In both nitrophorins and hydroxylamine oxidoreductase, a ruffled heme is proposed to increase the heme affinity for NO.[10,13] Ruffling also has been shown to modify heme electronic properties to facilitate enzymatic heme degradation by the enzymes heme oxygenase,[14] IsdI,[15] and MhuD.[16,17] In addition, ruffling is proposed to modulate the electronic coupling in a catalytic intermediate of nitrophorin 2, which has been discovered to have peroxidase functionality.[18] The heme in some cyano-protoglobins has been found to be highly ruffled, accounting for electronic structure differences with cyano-metmyoglobin.[19] The means by which heme ruffling modifies the electronic structure to influence function is not yet fully understood. Besides leading to a better understanding of structure−function relationships in heme proteins, understanding the impact of ruffling on metalloporphyrin properties is expected to enhance the development of metalloporphyrin-based catalysts.[20−24]

Most characterizations of heme conformation have relied on normal-coordinate structural decomposition (NSD) analysis of X-ray crystal structures, yielding the net out-of-plane displacement of porphyrin atoms along each distortion coordinate (i.e., ruffling, saddling, doming),[2] but recent efforts have focused on developing methods that reveal effects of the heme conformation on the electronic structure and function. For example, vibrational spectroscopy methods have been utilized to characterize heme out-of-plane distortions such as ruffling. Approaches include the use of resonance Raman marker frequencies,[25] Raman dispersion spectroscopy,[26] and femtosecond coherence spectroscopy.[27] Magnetic spectroscopy methods such as electron paramagnetic resonance (EPR) and NMR are well-suited to probe the interplay between heme geometric and electronic structure in paramagnetic heme proteins.[28−33] EPR has provided insight into the influence of ruffling on d-orbital energies,[34] and heme methyl ^{1}H shifts have

Received: May 17, 2013
Published: November 4, 2013

ACS Publications © 2013 American Chemical Society

dx.doi.org/10.1021/ic401250d | *Inorg. Chem.* 2013, 52, 12933−12946

been found to be sensitive to heme ruffling.[35,36] A recent study used NMR spectroscopy and density functional theory (DFT) calculations to investigate the effects of ruffling on heme electronic structure and proposed a mechanism for how ruffling affects heme redox properties.[5] Heme core ^{13}C NMR shifts have been used to determine the heme iron oxidation and spin state[37] and are being developed as probes of heme electronic structure.[5,38] For heme model complexes, ^{13}C shifts have been used to calculate the distribution of spin density on the porphyrin ring.[39] The spin densities determined from NMR provide a means by which to test molecular orbital models of heme electronic structure. Heme core ^{13}C shifts, however, have not yet been fully developed as probes of heme distortion. A goal of the work reported herein is to compare the use of ^{13}C and ^{1}H shifts of heme as probes of heme ruffling.

Cytochrome *c* has served as an ideal model for testing the influence of ruffling on heme properties.[5,6,34,40] The heme in cytochromes *c* tends to be highly ruffled, with little contribution from other types of out-of-plane distortions.[41] Additionally, the degree of ruffling can be modulated by site-directed mutagenesis without significantly disrupting the heme orientation within the protein structure[5,34] because the heme is covalently attached to the protein. Cytochromes *c* also tend to have a fixed axial histidine orientation,[8] simplifying the interpretation of spectroscopic data.[28] The present work aimed to measure the influence of ruffling on heme electronic structure in cytochromes *c* by analyzing ^{1}H and ^{13}C hyperfine NMR shifts. In this study, we compared heme ^{13}C and ^{1}H chemical shifts of wild-type and mutant cytochromes *c*, making use of mutants with established changes in ruffling relative to the wild type. One wild-type/mutant pair is *Pseudomonas aeruginosa* cytochrome c_{551} (*Pa* WT) and its point mutant with a more ruffled heme, *Pa* F7A. The ruffling of the *Pa* WT and *Pa* F7A hemes was previously characterized by X-ray crystallography, which showed that the F7A mutation nearly doubles the extent of ruffling, measured as the total out-of-plane displacement of heme atoms along the ruffling coordinate,[2] without significantly changing other out-of-plane deformations.[5,42,43] To include additional data points and evaluate another cytochrome *c*, we also measured and analyzed heme ^{1}H and ^{13}C chemical shifts for a series of *Hydrogenobacter thermophilus* cytochrome c_{552} variants, *Ht* M13V, *Ht* K22M, and *Ht* M13V/K22M, as well as the wild type (*Ht* WT). These mutations were previously determined by EPR to increase heme ruffling.[34] In addition to the heme resonances, we also included analyses of the His axial ligand chemical shifts. In the present study, the NMR hyperfine shifts were divided into contact and pseudocontact components using a simple model, allowing Fermi contact spin densities to be estimated. The results demonstrate how ruffling influences the spin density delocalization on the porphyrin and provide an illustration of the influence of ruffling on heme axial ligands. Furthermore, we demonstrate that the chemical shifts that are the most convenient to measure, the heme methyl ^{1}H shifts, provide the best NMR measure of the extent of ruffling.

■ MATERIALS AND METHODS

Protein Expression and Purification. The plasmid pSCH552 containing the gene for cytochrome c_{552} from *H. thermophilus* has previously been described[44] along with the mutants *Ht* M13V, *Ht* K22M, and *Ht* M13V/K22M.[45] The plasmid pETPA containing the gene to express *P. aeruginosa* cytochrome c_{551} has also been previously described[46] along with the *Pa* F7A variant.[34] Each of the cytochrome *c* genes was expressed in *Escherichia coli* BL21 Star (DE3) cells (Invitrogen) with the pEC86 plasmid containing the *ccmABCDEFGH* operon.[47] Growth in Luria−Bertani (LB) medium provided natural-isotope-abundance samples. Carbon-13 isotope enrichment of the core heme carbons was accomplished by expressing the protein in minimal medium supplemented with isotope-labeled 5-aminolevulinic acid (ALA), which is a biological precursor to heme.[48] Uniform ^{15}N labeling was accomplished by expression in minimal medium with $(^{15}NH_4)_2SO_4$ (Sigma-Aldrich) as the sole nitrogen source. The minimal medium recipe used has been reported elsewhere.[5] The 4-^{13}C and 5-^{13}C isotopically labeled ALA derivatives were synthesized according to literature methods.[49] *Ht* cytochromes *c*[44] and *Pa* cytochromes *c*[46] were purified as previously described. Concentrations were determined using extinction coefficients of $\varepsilon_{409.5}$ = 105 mM^{-1} cm^{-1} for ferric *Ht* cytochromes[44] and ε_{409} = 106.5 mM^{-1} cm^{-1} for ferric *Pa* cytochromes.[46,50]

NMR Spectroscopy. Oxidized (Fe^{III}) protein samples were obtained from purified protein exchanged into 50 mM NaP$_i$ buffer at pH 7.0, after which 10% D$_2$O and a 5-fold molar excess of $K_3Fe(CN)_6$ (Sigma-Aldrich) relative to protein were added. Reduced (Fe^{II}) samples were prepared by exchanging purified protein into 50 mM NaP$_i$ at pH 7.0 followed by lyophilization. The lyophilized sample was dissolved in 100% D$_2$O or 90% H$_2$O/10% D$_2$O under an argon atmosphere. A 10- to 20-fold excess of $Na_2S_2O_4$ (Sigma) was then added to reduce the sample, which was transferred to an NMR tube under a nitrogen atmosphere. Mixed-oxidation-state samples were prepared by partially oxidizing previously reduced samples by brief exposure to air. Final protein concentrations were 1−3 mM.

A 500 MHz Varian Inova spectrometer fitted with a triple-resonance probe was used for all NMR experiments. One-dimensional ^{1}H NMR spectra were recorded using presaturation of the water signal with a saturation delay of 1 s. ^{1}H−^{13}C heteronuclear multiple-quantum coherence (HMQC) spectra used to observe the heme methyl resonances were obtained with natural-isotope-abundance samples using a presaturation delay of 190 ms and a J_{CH} value of 200 Hz. ^{1}H−^{15}N heteronuclear single-quantum coherence (HSQC) spectra of ferric protein samples were obtained with uniformly ^{15}N-labeled protein samples using a J_{NH} value of 135 Hz; this high J_{NH} value enhances the detection of faster-relaxing nuclei.[45] A J_{NH} of 94 Hz was used for ^{1}H−^{15}N HSQC spectra of ferrous samples. 2D TOCSY spectra were collected using a spin-lock time of 90 ms, and 2D NOESY spectra were collected using a mixing time of 100 ms. A 3D HSQC-TOCSY spectrum was collected with uniformly ^{15}N-labeled ferrous *Ht* WT with a spin-lock time of 90 ms and a J_{NH} value of 94 Hz. Two-dimensional exchange spectroscopy (EXSY) was performed with a mixing time of 100 ms on mixed-oxidation-state samples. 1D ^{13}C experiments with ^{1}H decoupling were run on samples with core heme carbon isotope enrichment via labeling with [4-^{13}C]ALA or [5-^{13}C]ALA. For 1D ^{13}C experiments on Fe^{III} and Fe^{II} samples, recycle times of 120 ms and 2.3 s, respectively, were used. Data on *Pa* WT and *Pa* F7A were collected at 25 °C to facilitate comparison to published data on these and related proteins. However, data on *Ht* WT and its variants were collected at 40 °C because significant line broadening was observed for ^{13}C resonances for this protein at 25 °C, likely as a result of the fluxionality of the axial Met. All of the spectra were referenced to 4,4-dimethyl-4-silapentane-1-sulfonic acid (DSS) indirectly through the water resonance. One-dimensional spectra were processed with SpinWorks 3.1 beta using a 20 or 30 Hz line-broadening window function for ^{13}C and ^{1}H spectra, respectively. After phasing, peaks were fit to Lorentzian functions using the multipeak fitting package in Igor Pro 6.12. For 2D HMQC spectra, processing was performed with NMRPipe[51] using a previously published macro.[5]

Calculation of the metal-centered pseudocontact shifts for *Pa* WT and *Pa* F7A relied on the previously determined magnetic axes and anisotropic susceptibility of *Pa* WT.[32] The magnetic susceptibility values used are listed in Table S1 in the Supporting Information. Hydrogen atoms were added to each crystal structure using MolProbity.[52] The crystal structures were then oriented with the four pyrrole nitrogens of the heme in the *xy* plane, the +*z* axis pointing toward the axial methionine, and the iron at the origin. The molecule

Table 1. Chemical Shifts (ppm) for Oxidized *Pa* WT and *Pa* F7A[a]

	Pa WT	*Pa* F7A	(*Pa* F7A − *Pa* WT)	(*Ht* A7F − *Ht* WT)[b]
^{1}H methyl	22.10	21.35	−0.75	+0.17
^{13}C methyl	−41.0	−39.8	1.2	−0.9
^{1}H meso	2.64	2.58	−0.05	−0.13
^{13}C meso	37.0	38.2	+1.2	−0.5
α-pyrrole ^{13}C	29.4	29.3	−0.1	−4.9[d]
β-pyrrole ^{13}C[c]	141.7	140.5	−1.2	n.d.[e]
Met61 ε-C^{1}H$_3$	−16.91	−16.96	−0.05	−1.21
His16 δ_1-^{15}N	169.3	165.3	−4.0	n.d.[e]
His16 δ_1-N^{1}H	11.9	10.6	−1.30	n.d.[e]

[a] Data at 25 °C. Average chemical shifts are reported for heme nuclei. [b] Published data at 51 °C.[5] [c] Four out of the eight β-pyrrole ^{13}C shifts were averaged according to the [4-^{13}C]ALA labeling scheme (Figure 1a). [d] Data for four out of the eight α-pyrrole ^{13}C shifts according to the [5-^{13}C]ALA labeling scheme (Figure 1b). [e] Not determined.

Table 2. Chemical Shifts (ppm) for the Oxidized *Ht* Series of Variants[a,b]

	WT	K22M	M13V	M13V/K22M	(M13V/K22M − WT)[c]
^{1}H methyl	21.65	21.53	20.91	20.59	−1.06
^{13}C methyl	−36.7	−36.7	−36.4	−36.5	+0.2
^{1}H meso	3.63	3.58	3.26	3.18	−0.45
^{13}C meso	35.7	35.5	36.9	36.9	+1.1
α-pyrrole ^{13}C	53.9	54.1	44.8	41.9	−12.0
β-pyrrole ^{13}C[d]	158.9	157.4	151.0	146.7	−12.2
Met61 ε-C^{1}H$_3$	−15.27	−15.09	−17.69	−18.26	−2.99
His16 δ_1-^{15}N[e]	182.3	181.3	170.5	167.1	−15
His16 δ_1-N^{1}H[e]	13.2	12.6	11.8	11.2	−1.6

[a] Average chemical shifts are reported for heme nuclei. [b] The temperature was 40 °C except where noted otherwise. [c] The change in chemical shift for the most ruffled *Ht* variant relative to *Ht* WT. [d] Four out of the eight β-pyrrole ^{13}C shifts were averaged according to the [4-^{13}C]ALA labeling scheme (Figure 1a). [e] Measured at 25 °C, taken from ref 45.

was then rotated to place the heme pyrrole II nitrogen along the +*x* axis. The metal-centered pseudocontact shifts were then calculated according to literature procedures.[53] The orientation and anisotropy of the paramagnetic susceptibility tensor of *Ht* WT at 40 °C (pH 7.0) were determined herein from measured pseudocontact shifts. Chemical shift assignments for ferric *Ht* WT at 40 °C (pH 7.0) were made using TOCSY and NOESY spectra and by comparison to previous assignments at 25 °C (pH 5).[32] Assignments of ferrous *Ht* WT at 40 °C (pH 7.0) were made using TOCSY, NOESY, and 3D HSQC-TOCSY spectra and by comparison to previous assignments at both 25 °C (pH 5)[32] and 23 °C (pH 6).[54] Pseudocontact shifts were determined by taking the difference between the shifts in the oxidized and reduced states, using nuclei for which contact shift is negligible (i.e., excluding the heme, Cys12, Cys15, His16, and Met61). A total of 51 pseudocontact shifts were used in the fitting along with the resonance assignments in both oxidation states (Table S4). The magnetic axes determination used chain A of the 2.0 Å crystal structure of reduced *Ht* WT (PDB entry 1YNR).[55] Proton coordinates were added using MolProbity,[52] and the positions of the methyl protons were averaged over one rotation. The coordinate axes were defined as described above for *Pa* WT and *Pa* F7A. The fitting used methods and an in-house program described previously.[32] After determination of the magnetic axes orientation and magnetic anisotropies for *Ht* WT, pseudocontact shifts of the heme and axial ligand nuclei were calculated as described above for *Pa* WT and *Pa* F7A.

■ RESULTS AND ANALYSIS

NMR Assignments. *Heme Nuclei.* Heme ^{1}H and ^{13}C NMR assignments were made for ferric *Pa* WT, *Pa* F7A, *Ht* WT, *Ht* M13V, *Ht* K22M, and *Ht* M13V/K22M and are found in Tables 1 (*Pa* variants) and 2 (*Ht* variants). Heme and selected axial ligand ^{1}H and ^{13}C assignments made for reduced (diamagnetic) *Pa* WT are shown in Table S2. The heme assignments reported for reduced *Pa* WT were used as reference diamagnetic shifts throughout. The shifts of the four heme methyl substituents (Figure 1a) for all of the proteins were obtained via 1D ^{1}H and 2D ^{1}H−^{13}C HMQC

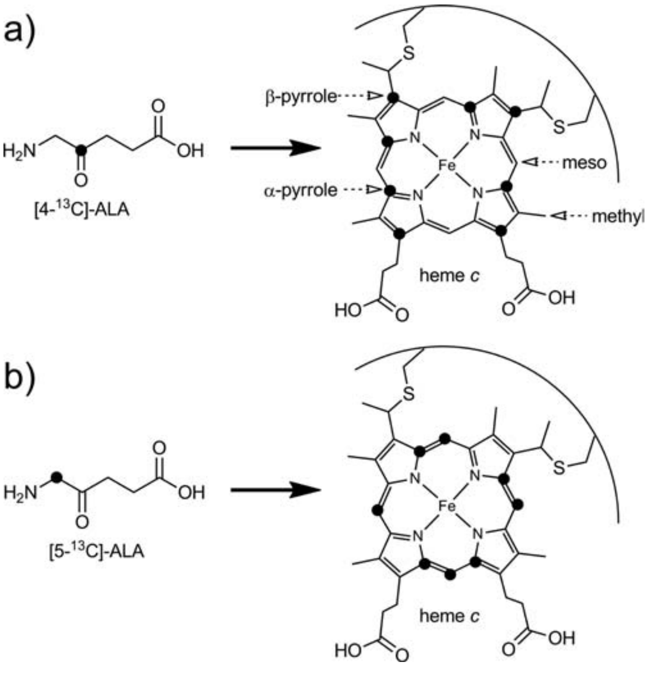

Figure 1. ^{13}C isotope labeling pattern obtained from the addition of (a) [4-^{13}C]ALA and (b) [5-^{13}C]ALA. Heme nuclei are labeled in (a).

spectra using samples at natural isotope abundance. In the oxidized proteins, the methyl resonances were identified in the 1D ^{1}H spectra as the most deshielded signals that integrated to three protons (Figures S1 and S2 in the Supporting Information), consistent with published assignments.[56] The methyl ^{13}C shifts were then obtained from cross-peaks in the ^{1}H−^{13}C HMQC spectra and were consistent with published assignments.[57] An overlay of the HMQC spectra of the *Ht* series of variants is shown in Figure S3, and an overlay of the *Pa* WT and *Pa* F7A spectra is shown in Figure S4. The meso ^{1}H and ^{13}C shifts were detected in ^{1}H−^{13}C HMQC spectra as well using the isotope labeling pattern provided by [5-^{13}C]ALA enrichment (Figure 1b). With this labeling pattern, the four meso carbons as well as four of the α-pyrrole carbons are ^{13}C-labeled. Since the meso carbons are the only isotopically enriched carbons with attached protons, these are the strongest signals in the HMQC spectra. HMQC spectra of [5-^{13}C]ALA-enriched samples are included in Figures S5−S7.

The α-pyrrole and β-pyrrole ^{13}C shifts were detectable only with 1D ^{13}C NMR. The four α-pyrrole carbons labeled with [5-^{13}C]ALA were identified in 1D spectra by eliminating the meso ^{13}C shifts assigned from the HMQC spectra. For *Pa* WT and *Pa* F7A, this assignment strategy was followed for both the Fe^{III} and Fe^{II} redox states (Figures S8−S12), with the exception that the reduced heme methyl ^{1}H shifts were obtained for *Pa* WT and *Pa* F7A by correlation cross-peaks observed in 2D EXSY spectra of mixed-oxidation-state samples (Figure S13). Heme chemical shifts for reduced *Pa* WT are given in Table S2.

Labeling of samples with [4-^{13}C]ALA yielded heme with four α-pyrrole and β-pyrrole carbons enriched with ^{13}C (Figure 1a). Distinguishing between the α-pyrrole and β-pyrrole resonances was made possible by the different labeling schemes and comparison to established chemical shift ranges for these nuclei in low-spin ferric heme.[38] A 1D ^{13}C spectrum of the [4-^{13}C]ALA-enriched sample of *Ht* WT (Figure 2d) shows four peaks between 10 and 70 ppm. These peaks are in the same chemical shift range as the α-pyrrole signals observed in the 1D ^{13}C spectrum of the [5-^{13}C]ALA-enriched *Ht* WT sample (Figure 2b) and were therefore assigned to α-pyrrole carbons. The remaining four peaks had chemical shifts larger than 120 ppm and thus were assigned to β-pyrrole carbons. This pattern, where α-pyrrole ^{13}C shifts are clustered with lower chemical shifts than the β-pyrrole ^{13}C shifts, has been previously observed in low-spin Fe^{III} heme proteins.[38]

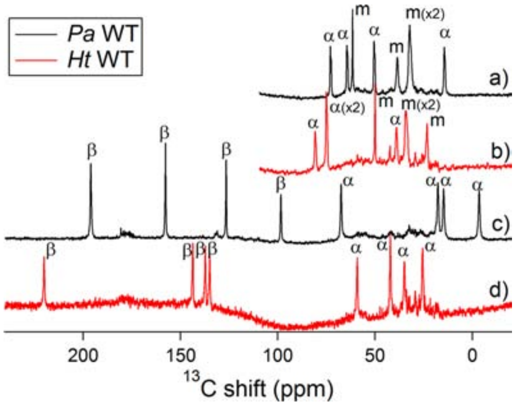

Figure 2. 1D ^{13}C NMR spectra of ferric heme resonances of *Pa* WT (black traces) and *Ht* WT (red traces): (a, b) spectra of [5-^{13}C]ALA-labeled samples of *Pa* WT and *Ht* WT, respectively; (c, d) spectra of [4-^{13}C]ALA-labeled samples of *Pa* WT and *Ht* WT, respectively.

For *Pa* WT and *Pa* F7A, this same general assignment strategy was employed to distinguish between the α-pyrrole and β-pyrrole signals of the [4-^{13}C]ALA-labeled samples (Figure S11). The four α-pyrrole ^{13}C signals from the [5-^{13}C]ALA-labeled sample are between −5 and +75 ppm. For both *Pa* WT and *Pa* F7A, there are only four peaks from the [4-^{13}C]ALA-labeled samples that appear in this region; these were assigned to the α-pyrrole carbons. The remaining four signals, which have chemical shifts greater than 90 ppm, were then assigned to β-pyrrole carbons. Using this assignment strategy with *Pa* WT and *Pa* F7A leaves some doubt in differentiating between the α- and β-pyrrole carbons in the [4-^{13}C]ALA-labeled samples. In *Pa* WT, the chemical shift of the most shielded β-pyrrole is less than 25 ppm higher than the least shielded α-pyrrole carbon. This is in contrast with the more than 65 ppm separation found in the *Ht* variants. The decreased separation between the α- and β-pyrrole carbon shifts in the *Pa* variants increases the likelihood of an overlap between their chemical shift ranges. For example, in the case of *Pa* WT, the peaks at 63.9 and 90.9 ppm (25 °C, Figure 2c) have a chance of being assigned incorrectly. To resolve this ambiguity, temperature dependences of the α- and β-pyrrole carbon shifts were measured for *Pa* WT and *Pa* F7A. Hyperfine shifts in cytochromes *c* do not typically exhibit standard Curie behavior because of the presence of a thermally accessible excited state.[33] As a consequence, Curie plots of hyperfine shifts have *y*-intercepts that deviate from the diamagnetic shift values. Since the atypical Curie behavior is well-understood for cytochromes *c*, an analysis of the temperature dependence assists in the assignment of the core heme carbons.

The temperature dependence of the α- and β-pyrrole carbon shifts of *Pa* WT is shown in Curie plots in Figure 3. The diamagnetic reference shifts were determined via ^{13}C NMR of the [4-^{13}C]- and [5-^{13}C]ALA-labeled samples of *Pa* WT in the Fe^{II} redox state (Figure S12 and Table S2). The average diamagnetic ^{13}C shifts for the α-pyrroles and β-pyrroles were 147.7 and 144.8 ppm, respectively. These values were subtracted from the observed chemical shifts to estimate the hyperfine shifts, which are plotted on the *y* axis in Figure 3. A decrease in the magnitude of the hyperfine shift with increasing temperature and a *y*-intercept of zero would thus be standard Curie behavior. As can be seen in Figure 3, the *Pa* WT peak at 90.9 ppm (25 °C) exhibits hyper-Curie behavior while the peak at 63.9 ppm exhibits hypo-Curie behavior. A pattern in the temperature dependence of cytochrome *c* methyl ^{1}H and ^{13}C shifts has been previously observed in which the more hyperfine-shifted peaks exhibit hyper-Curie behavior and the less hyperfine-shifted peaks exhibit hypo- or anti-Curie behavior.[33] The reason for this behavior is a shift in the Boltzmann population of the low-lying excited state. It is expected that the temperature dependence of the β-pyrrole ^{13}C shifts follow the same pattern as the heme methyl resonances because the paramagnetic shifts of the heme methyl resonances are mostly a result of the polarization of spin density from the β-pyrrole carbons. The temperature dependence of the resonances at 63.9 and 90.9 ppm is consistent with this pattern only if they are assigned as α-pyrrole and β-pyrrole signals, respectively. The same temperature dependence study was used to clarify the assignments of *Pa* F7A and is shown in Figure S14.

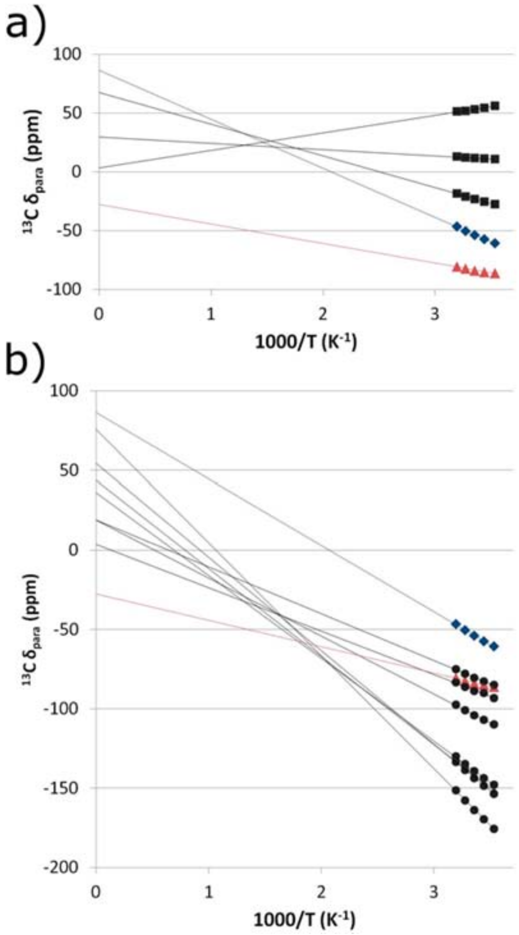

Figure 3. (a) Temperature dependence of the three unambiguously assigned β-pyrrole ^{13}C shifts for *Pa* WT (black squares) compared with that of the two peaks with ambiguous assignments (blue diamonds, red triangles). (b) Temperature dependence of the seven unambiguously assigned α-pyrrole ^{13}C shifts for *Pa* WT (black circles) compared with that of the two peaks with ambiguous assignments (blue diamonds, red triangles). In both (a) and (b), the blue diamonds represent the peak tentatively assigned to a β-pyrrole carbon on the basis of its lower shift and temperature dependence, while the red triangles represent the peak tentatively assigned to an α-pyrrole carbon.

Axial Ligands. Axial ligand assignments were made by comparison to previous assignments.[58] The only significantly hyperfine-shifted resonance in the HSQC spectra of *Pa* WT and *Pa* F7A is that of the δ_1-NH of the heme axial His16.[45] An overlay of the HSQC spectra with the δ_1-NH signals evident is shown in Figure S15. The axial methionine ε-CH_3 peak can be observed in a 1D ^1H spectrum as the only peak with a chemical shift lower than −10 ppm that integrates to three protons (Figures S1 and S2). Chemical shift assignments are shown in Tables 1 and 2.

Chemical Shift Changes with Ruffling.

Pa Cytochrome c_{551} Variants. The heme in *Pa* F7A has been shown by X-ray crystallography to be more ruffled than the heme in *Pa* WT.[43] The heme ^1H and ^{13}C NMR shifts were recorded for both *Pa* WT and *Pa* F7A to learn the effect of ruffling on these shifts. In addition, the axial methionine ε-CH_3 ^1H shift was measured along with the axial His δ_1-^{15}N and δ_1-N^1H shifts (Figure 4). Table 1 reports the chemical shifts for *Pa* F7A compared with *Pa* WT and compares the chemical shift differences between *Pa* F7A and *Pa* WT to those between *Ht* A7F and *Ht* WT, which have previously been published.[5] The use of average chemical shift values for each type of heme nucleus minimizes the effect of asymmetric spin density distributions that result from the axial ligand interactions with heme and allows an analysis despite the lack of atom-specific assignments of heme core carbons.

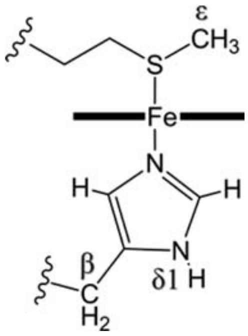

Figure 4. Diagram of the axial ligands of cytochrome *c* showing labels for nuclei relevant to this work.

The heme chemical shifts of *Pa* F7A show a number of differences from those of *Pa* WT. In the more-ruffled *Pa* F7A, the magnitudes of the average heme methyl ^{13}C and ^1H shifts decrease relative to those of *Pa* WT. Second, the average heme meso ^{13}C shift increases while the average heme meso ^1H shift decreases slightly. The average of the four measured β-pyrrole shifts decreases slightly, as does the average of all eight α-pyrrole shifts. These changes in average chemical shifts in *Pa* F7A relative to *Pa* WT are reported in Table 1, where they are compared with previously published chemical shift changes observed for *Ht* A7F, a mutation that slightly decreases the extent of heme ruffling.[5] The influence of heme ruffling is predicted to change the chemical shifts of *Pa* F7A relative to *Pa* WT in the opposite direction as that observed for *Ht* A7F relative to *Ht* WT in published work.[5] As expected, the ^1H methyl, ^{13}C methyl, and ^{13}C meso chemical shift changes in *Pa* F7A are in the opposite directions of those previously reported for *Ht* A7F. However, on the basis of the *Ht* A7F results, while the average α-pyrrole shift was expected to increase with ruffling for *Pa* F7A, the average α-pyrrole shift slightly decreased. Likewise, the average ^1H meso shift moved in the same direction in *Pa* F7A as in *Ht* A7F relative to the wild-type proteins. Finally, the axial ligand chemical shifts of *Pa* WT and *Pa* F7A were compared. As can be seen in Table 1, the axial methionine (Met61) ε-C^1H_3 resonance shifts to lower frequency in *Pa* F7A relative to *Pa* WT, but only slightly. On the proximal side of the heme, the axial His (His16) δ_1-^{15}N and δ_1-N^1H resonances shift to lower frequency in *Pa* F7A (Table 1).

Ht Cytochrome c_{552} Variants. The series of *Ht* variants studied was chosen on the basis of a previous EPR study showing that heme ruffling increases in the following order: WT < K22M < M13V < M13V/K22M.[34] NMR chemical shift data for the heme core ^{13}C meso, α-pyrrole, and β-pyrrole shifts were collected on all four *Ht* variants. Chemical shifts of selected heme substituents were also measured, including the ^{13}C-methyl, ^1H methyl, and ^1H meso chemical shifts. The axial methionine (Met61) ε-C^1H_3 shift may be influenced by ruffling, as suggested by DFT studies,[5] and was measured as well. All of the above-mentioned measured chemical shifts are strongly correlated to each other across this series of *Ht* mutants. As ruffling increases across the series, the ^{13}C meso and ^{13}C methyl nuclei are deshielded, while the ^{1}H meso, ^{1}H methyl, ^{13}C α-pyrrole, ^{13}C β-pyrrole, and Met ε-C^{1}H$_3$ shifts become more shielded. These results can be seen in Figure 5, where the difference in the chemical shifts for each of these resonances relative to *Ht* WT is plotted versus the EPR axial term, Δ/λ, of each variant. Previous work has shown that as long as other factors that influence the ligand-field parameters are not significantly perturbed, the ligand-field parameters for low-spin cytochromes *c* with His/Met axial ligation correlate well with the amount of ruffling, with the axial term decreasing as the ruffling increases.[34] The factors expected to change the ligand-field parameters the most are the type and orientation of the heme axial ligands,[59] which are maintained among these mutants, as revealed by the crystal structures of *Pa* WT[42] and *Pa* F7A[55] as well as NMR data on the *Ht* variants.[45,58] Notably, a similar correlation between the ligand-field parameters and heme ruffling has been noted in cyanide-inhibited globins.[19] In Figure 5, it is apparent that all of the changes observed in the chemical shifts of the more-ruffled *Ht* variants relative to the less-ruffled variants are in the same direction as those observed in the more-ruffled *Pa* F7A relative to *Pa* WT. This observation demonstrates consistency in the way in which ruffling influences the NMR chemical shifts in these *Ht* and *Pa* variants. The chemical shift data for the *Ht* series of mutants are shown in Table 2.

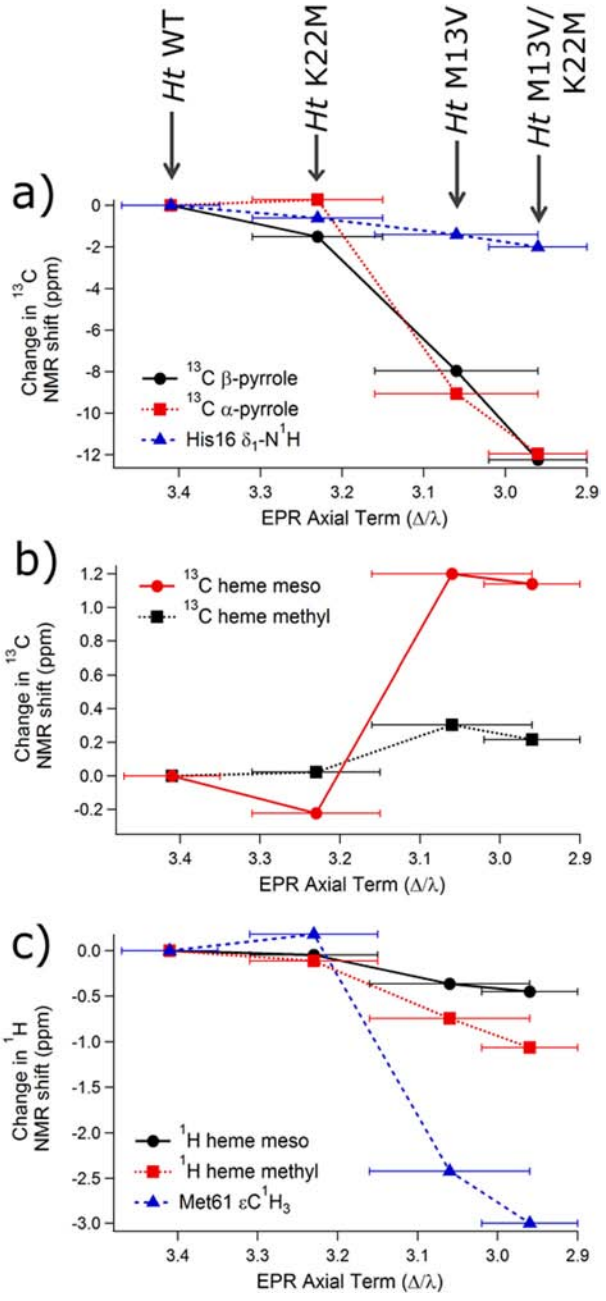

Figure 5. Chemical shift differences associated with the *Ht* K22M, *Ht* M13V, and *Ht* M13V/K22M variants relative to WT. Each point represents the value of δ(mutant) − δ(wild-type). Ruffling increases as the EPR axial term decreases (left to right). The His16 β-^{13}C chemical shifts are reported in ref.[58] and the EPR parameters and associated errors are reported in ref.[34]

Analysis of Chemical Shifts. The chemical shift of a nucleus in a paramagnetic species can be expressed as the sum of the diamagnetic shift (δ_{dia}), which is the chemical shift in the absence of any influence from the unpaired electron(s), and the paramagnetic shift (δ_{para}), which is a result of the hyperfine interaction between the nucleus and the unpaired electron spin:

$$\delta_{\text{obs}} = \delta_{\text{dia}} + \delta_{\text{para}} \tag{1}$$

For low-spin cytochromes that do not undergo significant redox-triggered structural rearrangements, the diamagnetic shift can be approximated by the chemical shift of the Fe$^{\text{II}}$ species. The paramagnetic shift can further be described in terms of a through-space metal-centered pseudocontact term ($\delta_{\text{PC}}^{\text{MC}}$), a through-bond Fermi-contact term (δ_{FC}), and a through-space ligand-centered pseudocontact term ($\delta_{\text{PC}}^{\text{LC}}$):

$$\delta_{\text{para}} = \delta_{\text{PC}}^{\text{MC}} + \delta_{\text{FC}} + \delta_{\text{PC}}^{\text{LC}} \tag{2}$$

The metal-centered pseudocontact shift depends on the nuclear coordinates in the three-dimensional magnetic axes of the metal center, which are largely determined by the orientation of the axial ligands with respect to the heme, and on the magnetic anisotropy.[29] The metal-centered pseudocontact shift is described by the following equation:[60,61]

$$\delta_{\text{PC}}^{\text{MC}} = \frac{1}{12\pi r^3}\left[\Delta\chi_{\text{ax}}(3\cos^2\theta - 1) + \frac{3}{2}\Delta\chi_{\text{rh}}\sin\theta\cos 2\phi\right] \tag{3}$$

in which $\Delta\chi_{\text{ax}}$ and $\Delta\chi_{\text{rh}}$ are the axial and rhombic paramagnetic anisotropies, respectively, and r, θ, and ϕ are the polar coordinates of the nucleus in the reference frame of the magnetic axes. For nuclei many bonds from the metal center (i.e., excluding the heme and axial ligands), the paramagnetic shift consists solely of a metal-centered pseudocontact component:

$$\delta_{\text{PC}}^{\text{MC}} = \delta_{\text{para}} - \delta_{\text{dia}} \tag{4}$$

The metal-centered pseudocontact shift can then be calculated for any nucleus using δ_{para} values, the protein structure, the magnetic axes, and the values of $\Delta\chi_{\text{ax}}$ and $\Delta\chi_{\text{rh}}$ according to eq 3. For *Pa* WT and *Ht* WT, the crystal structures[42,55] and the paramagnetic susceptibility tensors[32] at 25 °C have been previously determined, allowing for the calculation of the pseudocontact shifts for all of the heme and axial ligand nuclei. Pseudocontact shifts were calculated for heme nuclei of *Pa* WT, and the results were averaged for each type of heme nucleus (i.e., β-pyrrole ^{13}C, α-pyrrole ^{13}C, meso ^{1}H, etc.; Table 3). This

Table 3. Contributions to the Paramagnetic Chemical Shifts (ppm) of the Heme and Axial Ligands of *Pa* WT and *Pa* F7A[a]

	Pa WT			*Pa* F7A		
	δ_{para}	$\delta_{\text{PC}}^{\text{MC}}$	$\delta_{\text{FC}} + \delta_{\text{PC}}^{\text{LC}}$	δ_{para}	$\delta_{\text{PC}}^{\text{MC}}$	$\delta_{\text{FC}} + \delta_{\text{PC}}^{\text{LC}}$
^{1}H methyl	18.55	−2.87	21.42	17.86	−2.73	20.59
^{13}C methyl	−55.7	−4.7	−50.9	−54.5	−4.5	−50.0
^{1}H meso	−6.91	−8.41	1.50	−6.97	−7.60	0.63
^{13}C meso	−62.7	−19.6	−43.1	−61.5	−18.2	−43.3
^{13}C α-pyrrole	−118.3	−27.7	−90.6	−118.5	−26.2	−92.3
^{13}C β-pyrrole	−3.1	−10.0	6.9	−4.3	−9.1	4.8
Met61 ε-C^{1}H$_{3}$	−13.99	10.04	−24.03	−14.04	9.78	−23.82
His16 δ_{1}-^{15}N	48.9	19.8	29.1	44.9	19.6	25.3
His 16 δ_{1}-N^{1}H	5.17	10.0	−4.85	3.87	9.7	−5.87

[a] Average chemical shifts are reported for heme nuclei.

same calculation has been performed previously for the heme methyl nuclei of *Ht* WT[58] and horse cytochrome *c*.[33]

Because the paramagnetic susceptibility tensor of *Ht* WT had been previously determined at 25 °C,[32] the tensor was determined here at 40 °C using experimentally determined pseudocontact shifts for *Ht* WT (Table S4). A plot of the calculated versus observed metal-centered pseudocontact shifts is shown in Figure S16. The magnetic axes orientation, given in Table S1, changed minimally from that determined at 25 °C. The anisotropy terms in Table S1 decreased in magnitude relative to those at 25 °C, as expected for an increase in temperature. The results of the determination of the pseudocontact shifts at 40 °C for the heme and axial ligand nuclei of *Ht* WT and variants using the magnetic axis parameters are shown in Tables S5 and S6.

The Fermi contact term is significant only for nuclei of the axial ligands and the heme. For unpaired electron density delocalized in a π-system, the Fermi contact shift is increased by positive spin density on the measured nucleus and decreased by positive spin density on adjacent nuclei. The Fermi contact shift is determined by the following relationship:[33,62]

$$\delta_{\text{FC}} = \frac{A^{\text{H}}\beta g S(S+1)}{\gamma_{I}\hbar 3k_{\text{B}}T} \tag{5}$$

in which A^{H} is the hyperfine coupling constant, which can be related to the spin density using empirical proportionality constants that have been determined using organic radicals.[63] In heme, the terms used depend on the nucleus as follows:

$$A^{\text{H}}(^{1}\text{H}_{\text{meso}}) = \frac{Q_{\text{CH}}^{\text{H}}\rho_{\text{meso}}^{\pi}}{2S} \tag{6}$$

$$A^{\text{H}}(^{13}\text{C}_{\text{methyl}}) = Q_{\text{C}'\text{C}}^{\text{C}}\rho_{\beta}^{\pi}/2S \tag{7}$$

$$A^{\text{H}}(^{13}\text{C}_{\text{meso}}) = [(S^{\text{C}} + 2Q_{\text{CC}'}^{\text{C}} + Q_{\text{CH}}^{\text{C}})\rho_{\text{meso}}^{\pi} + 2Q_{\text{C}'\text{C}}^{\text{C}}\rho_{\alpha}^{\pi}]/2S \tag{8}$$

$$A^{\text{H}}(^{13}\text{C}_{\beta}) = \left[(S^{\text{C}} + 3Q_{\text{CC}'}^{\text{C}} + Q_{\text{C}'\text{C}}^{\text{C}})\rho_{\beta}^{\pi} + Q_{\text{C}'\text{C}}^{\text{C}}\rho_{\alpha}^{\pi}\right]/2S \tag{9}$$

$$A^{\text{H}}(^{13}\text{C}_{\alpha}) = \left[(S^{\text{C}} + 2Q_{\text{CC}'}^{\text{C}} + Q_{\text{CN}}^{\text{C}})\rho_{\alpha}^{\pi} + Q_{\text{C}'\text{C}}^{\text{C}}\rho_{\beta}^{\pi} + Q_{\text{C}'\text{C}}^{\text{C}}\rho_{\text{meso}}^{\pi} + Q_{\text{NC}}^{\text{C}}\rho_{\text{N}}^{\pi}\right]/2S \tag{10}$$

In the above equations, ρ_{meso}^{π}, ρ_{β}^{π}, ρ_{α}^{π}, and ρ_{N}^{π} are the spin densities on the meso carbon, β-pyrrole carbon, α-pyrrole carbon, and pyrrole nitrogen, respectively. The values for the proportionality constants used[63] can be found in Table S3. If multiple Fermi contact shifts of the heme nuclei are known, the above eqs 6−10 can be combined with eq 5 and simultaneously solved to estimate the spin density distribution on the core heme nuclei, as has been performed before for other iron porphyrins.[39,64,65] It is important to note that eqs 6−10 are derived from simple models, assuming no deviations from the Curie law and only π-delocalization of the unpaired electron onto the porphyrin ligand. Therefore, the results should be considered to be qualitative in nature.

For ferricytochrome *c*, the ligand-centered pseudocontact shifts are insignificant for most of the protein because the spin density lies primarily at the iron. However, for nuclei on which there is delocalized spin density, including the porphyrin core nuclei and some of the axial ligand nuclei, the ligand-centered pseudocontact shift can be significant.[39] The shift is approximately proportional to the spin density at the measured nucleus. This relationship is expressed using an empirical proportionality constant, *D*:[39,66]

$$\delta_{\text{PC}}^{\text{LC}} = D\rho_{I}^{\pi} \tag{11}$$

The presence of a ligand-centered pseudocontact shift necessitates the use of an additional term when fitting the ^{13}C meso, ^{13}C α-pyrrole and ^{13}C β-pyrrole shifts, since for these nuclei $\delta_{\text{PC}}^{\text{LC}}$ is significant:

$$\delta_{\text{para}} - \delta_{\text{dia}} - \delta_{\text{PC}}^{\text{MC}} = \delta_{\text{FC}} + \delta_{\text{PC}}^{\text{LC}} \tag{12}$$

Therefore, to fit the spin densities, the equation for the ^{13}C meso shift combines eqs 5, 8, and 11 and is shown below (eq 13):

$$(\delta_{\text{FC}} + \delta_{\text{PC}}^{\text{LC}})_{\text{meso}} = \left[\left(\frac{\beta g S(S+1)}{\gamma_{I}\hbar 3k_{\text{B}}T}\right)(S^{\text{C}} + 2Q_{\text{CC}'}^{\text{C}} + Q_{\text{CH}}^{\text{C}}) + D\right]\rho_{\text{meso}}^{\pi} + \left(\frac{\beta g S(S+1)}{\gamma_{I}\hbar 3k_{\text{B}}T}\right)(2Q_{\text{C}'\text{C}}^{\text{C}}\rho_{\alpha}^{\pi}) \tag{13}$$

The equations for the ^{13}C α-pyrrole and ^{13}C β-pyrrole shifts (eqs S1 and S2 in the Supporting Information) have analogous modifications to include the ligand-centered pseudocontact term.

By means of the above analysis, the spin density on the core heme carbons can be determined using the chemical shifts for the Fe$^{\text{III}}$ and Fe$^{\text{II}}$ states, accounting for the pseudocontact shift components. For the analysis, the four heme methyl ^{1}H shifts were averaged, as were the four ^{13}C heme methyl shifts, the four ^{1}H and ^{13}C meso shifts, four of the eight β-pyrrole ^{13}C shifts, and the eight α-pyrrole ^{13}C shifts. Averaging the NMR chemical shifts for each atom type minimizes the influence of an asymmetric distribution of spin densities around the heme and allows analysis without atom-specific chemical shift assignments. Only four of the eight β-pyrrole ^{13}C shifts were collected and averaged from the sample enriched with [4-^{13}C]ALA. The other four β-pyrrole ^{13}C shifts would have required a different labeling scheme using an ALA derivative that was not readily accessible at the time that the measurements were made. Atom-specific assignments, although possible,[67] would be difficult and would add unnecessary complexity to the analysis.

The results of this analysis performed for *Pa* WT are presented in Table 4, where a value for *D*, the proportionality constant from eq 11, was determined from the fit to the data set. In addition, the same analysis was performed on the chemical shift changes associated with introducing the mutation to prepare the more ruffled *Pa* F7A variant, using the same value for *D* that was determined for *Pa* WT. The results show the change in spin density associated with the 0.4 Å increase in ruffling of the *Pa* F7A variant. The results are represented pictorially in Figure 6. The same analysis was also performed for *Ht* WT while also using a best fit value for *D*. The resulting spin densities are shown in Table 5 along with spin density changes associated with each of the *Ht* variants, using the value for *D* determined from *Ht* WT. The spin density changes are graphed in Figure 7.

Table 4. Calculated Average Spin Densities for Selected Heme Nuclei of *Pa* WT and Comparison to *Pa* F7A

	Pa WT	(F7A − WT)
meso ^{13}C	−0.00090	4.3×10^{-4}
β-pyrrole ^{13}C	0.012	-2.1×10^{-4}
α-pyrrole ^{13}C	0.0044	4.2×10^{-4}
N-pyrrole ^{13}C	0.017	8.1×10^{-4}

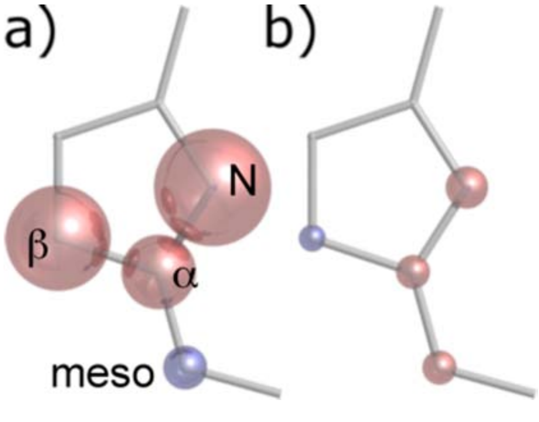

Figure 6. Graphical representation of the predicted average spin densities on the α-pyrrole carbon, β-pyrrole carbon, meso carbon, and pyrrole nitrogen. Red and blue represent positive and negative spin densities, respectively. The volumes of the glossy spheres are proportional to (a) the empirically calculated spin densities in *Pa* WT and (b) the spin density changes associated with the F7A mutation. The pyrrole nitrogen is predicted in other studies to have a mixture of positive and negative spin density, with an excess of negative spin density. See the text for discussion.

DISCUSSION

Relation to Previous Studies of Ruffled Hemes. Heme hyperfine shifts have previously been shown to reflect heme ruffling. In particular, the average heme methyl ^{1}H shift has been shown to decrease as ruffling increases in nitrophorins and cytochromes.[35,36] In a study that analyzed the heme chemical shifts in *Ht* WT relative to a less ruffled variant, *Ht* A7F,[5] several hyperfine shifts for the A7F variant were found to change predictably with the decrease in heme ruffling caused by the mutation, although the effect of the mutation on the ruffling was quite small (0.05−0.1 Å decrease in the out-of-plane displacement of porphyrin ring atoms along the ruffling coordinate). DFT calculations assisted in the interpretation of the NMR results, providing a molecular orbital interpretation of the effects of heme ruffling on the chemical shifts. Overall, the study developed the use of NMR of heme nuclei as a qualitative probe of heme ruffling and supported the hypothesis that increasing ruffling decreases the heme reduction potential.[5]

In the current study, NMR was performed on four variants of *Ht* cytochrome c_{552}: WT, K22M, M13V, and M13V/K22M; the three mutants have all been shown by EPR and NMR spectroscopy to have increased heme ruffling compared with the WT, although the amount of change has not been determined.[34] Second, NMR of *Pa* WT, along with a structurally characterized more ruffled variant, *Pa* F7A, was performed. The X-ray crystal structure of *Pa* F7A shows that heme ruffling has a magnitude of 0.86 Å in this mutant, compared with 0.49 Å for the wild type.[42,43] The results here are broadly consistent with previous work. The heme methyl and heme meso ^{1}H shifts move to lower frequency with increased ruffling, and the heme methyl and heme meso ^{13}C shifts move to higher frequency with increased ruffling (Figure 5, Table 1, and Table 2). However, although there is broad agreement, a few shift changes deviate from what was seen in the previous study on the *Ht* WT/*Ht* A7F pair. The axial Met ε-C^{1}H$_3$ shift and the α-pyrrole ^{13}C shift were introduced as potential probes of ruffling in the previous study on *Ht* A7F, and both shifts were observed to increase with an increase in ruffling.[5] DFT calculations performed on a heme model reproduced the same increase in chemical shift with ruffling. However, in the current study, the more ruffled variants (the three *Ht* variants and the *Pa* F7A variant) displayed decreased Met ε-C^{1}H$_3$ and α-pyrrole ^{13}C shifts. These results suggest that complex factors determine the Met ε-C^{1}H$_3$ shift and the α-pyrrole ^{13}C shift. Variations in axial ligand strength related to the mutations or to ruffling are a factor that may complicate the results.

In order to elucidate the complex relationships between heme NMR shifts and ruffling, it is helpful to factor out components contributing to the hyperfine shift. The separation of metal-centered pseudocontact shifts from the contact and ligand-centered pseudocontact shifts has been performed here and allows a detailed determination of the factors influencing changes in spin density when the ruffling is changed. The analysis also determines how the spin density components for each type of porphyrin nucleus contribute to the chemical shift. The pseudocontact shifts for the mutants were determined using the variants' *g* values reported previously[5,34] to scale the magnetic axis parameters for the wild-type proteins, which were determined previously for *Pa* WT[32] and herein for *Ht* WT.

Table 5. Calculated Average Spin Densities for Selected Heme Nuclei of *Ht* WT as Well as the Changes in Spin Density between *Ht* WT and Its Variants

	Ht WT	(K22M − WT)	(M13V − WT)	(M13V/K22M − WT)
meso ^{13}C	−0.0011	$+3.3 \times 10^{-4}$	$+16 \times 10^{-4}$	$+24 \times 10^{-4}$
β-pyrrole ^{13}C	0.011	$+0.4 \times 10^{-4}$	-1.0×10^{-4}	-1.3×10^{-4}
α-pyrrole ^{13}C	0.0044	$+4.2 \times 10^{-4}$	$+20 \times 10^{-4}$	$+30 \times 10^{-4}$
N-pyrrole ^{15}N	0.015	$+8.1 \times 10^{-4}$	$+49 \times 10^{-4}$	$+69 \times 10^{-4}$

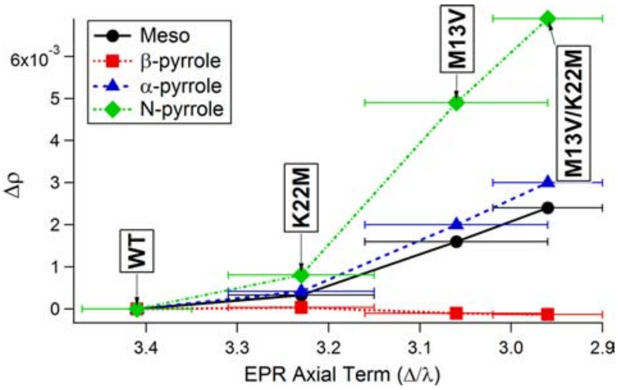

Figure 7. Calculated Average Spin Density Changes ($\Delta\rho$) Relative to the Wild Type for the Variants of *Ht* Cytochrome c_{552} Plotted against the EPR Axial Term for Each Type of Core Porphyrin Nuclei[34]

Diamagnetic reference shifts are shown in Table S2. Results for *Pa* WT and F7A are shown in Tables 6 and 7, while results for the *Ht* variants are shown in Tables S7−S10.

Table 6. Contributions to the Sum of the Average Contact and Ligand-Centered Pseudocontact Shifts (ppm) for Selected Heme Nuclei of *Pa* WT[a]

	ρ^{π}_{meso}	$\rho^{\pi}_{\beta\text{-pyrrole}}$	$\rho^{\pi}_{\alpha\text{-pyrrole}}$	$\rho^{\pi}_{\text{N-pyrrole}}$
^{1}H meso	1.5	–	–	–
^{13}C methyl	–	−50.9	–	–
^{13}C meso	−6.9	–	−36.2	–
^{13}C β-pyrrole	–	25.0	−18.1	–
^{13}C α-pyrrole	3.7	−50.9	27	−70.4

[a]The contributions from the spin density on each of the nuclei are shown independently. The data shown are for *Pa* WT at 25 °C in units of ppm.

Table 7. Contributions to the Chemical Shift Difference (ppm) between *Pa* F7A and *Pa* WT, (*Pa* F7A − *Pa* WT)[a]

	ρ^{π}_{meso}	$\rho^{\pi}_{\beta\text{-pyrrole}}$	$\rho^{\pi}_{\alpha\text{-pyrrole}}$	$\rho^{\pi}_{\text{N-pyrrole}}$
^{1}H meso	−0.71	–	–	–
^{13}C methyl	–	0.87	–	–
^{13}C meso	3.26	–	−3.42	–
^{13}C β-pyrrole	–	−0.43	−1.71	–
^{13}C α-pyrrole	−1.76	0.87	2.55	−3.34

[a]The values take only the contributions from the contact and ligand-centered pseudocontact shifts for heme ^{1}H and ^{13}C nuclei. The total shift difference (*Pa* F7A − *Pa* WT) is divided according to the contributions that arise from spin density on each of the four types of porphyrin core nuclei. The data shown were calculated using the difference in chemical shifts of *Pa* F7A and *Pa* WT at 25 °C in units of ppm.

Porphyrin Spin Densities. The spin density pattern on the porphyrin macrocycle of *Pa* WT (Table 4) agrees well with that of *Ht* WT (Table 5). The spin densities determined here also show broad agreement with analysis of spin density on a meso-substituted, low-spin Fe$^{\text{III}}$−porphyrin with two axial 1-methylimidazole ligands.[39] Large and positive spin densities are found on the β-pyrrole carbons, a moderate positive spin density is seen on the α-pyrrole carbons, and a small negative density is seen on the meso carbons for both proteins here (Tables 4 and 5 and Figure 6). This agreement, along with the general robustness of the results to potential sources of error (described below), provides confidence in the qualitative interpretation of the values obtained.

The changes observed for the porphyrin spin densities as a result of increased ruffling were estimated for *Pa* F7A relative to the WT (Table 4) as well as for the series of more ruffled *Ht* variants (Table 5). The changes are consistent between the two cytochromes, with the only notable difference being that the *Ht* variants with increased ruffling display greater increases of spin density on the meso carbon, α-pyrrole carbon, and pyrrole nitrogen than is seen for the *Pa* WT/*Pa* F7A pair. The observed trend between heme ruffling and empirical spin density changes can be partially understood within the framework of an existing molecular orbital (MO) interpretation of ruffling.[5,37,68] In cytochromes *c*, the unpaired electron primarily lies in one of the iron d_{π} orbitals (d_{xz} or d_{yz}), with the singly occupied d_{π} orbital being thermally accessible.[33] The iron d_{π} and porphyrin $3e_g$ orbitals (Figure 8) have the same

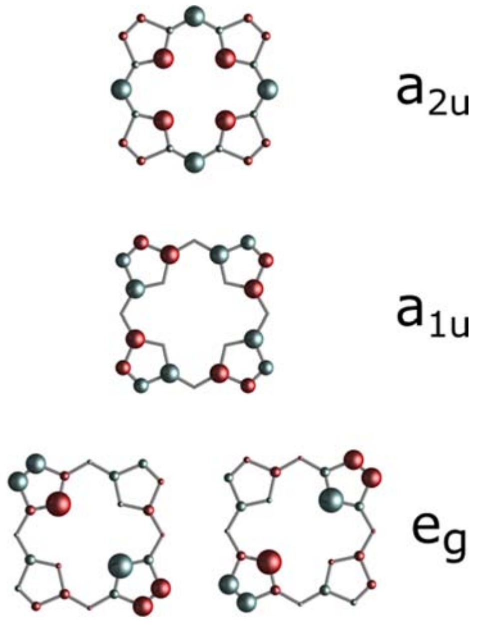

Figure 8. Graphical representation of porphyrin orbitals showing that the e_g orbital density is primarily on the β-pyrrole carbons and pyrrole nitrogens while the a_{2u} orbital density is primarily on the meso carbons and pyrrole nitrogens. The area of each circle is proportional to the Hückel coefficient generated with MPORPHW.[73]

symmetry, resulting in spin delocalization into the π-system to the porphyrin β-pyrrole carbons. Ruffling of the porphyrin raises the energy of the iron d_{xy} orbital relative to the d_π orbitals and consequently yields an increase in d_{xy} character of the singly occupied molecular orbital (SOMO), which has been observed by EPR.[34,37] The iron d_{xy} and porphyrin $3a_{2u}$ orbitals (Figure 8) have the same symmetry (b_2) in a ruffled (D_{2d}) heme, resulting in a slightly different spin delocalization pattern on the porphyrin for ruffled versus planar hemes. The porphyrin $3e_g$ orbital will have less spin density as ruffling is increased, resulting in a decrease in the β-pyrrole carbon spin density. Also, the $3a_{2u}$ orbital will have more spin density, resulting in increased meso carbon spin density.

This molecular orbital framework is consistent with the changes observed here in the spin densities of more ruffled variants of both *Pa* and *Ht* cytochromes *c*. As the ruffling is increased, the spin densities on the β-pyrrole and meso carbons decrease and increase, respectively, as predicted. The results also indicate that with increased ruffling, the spin densities on the α-pyrrole carbons increase. This experimental result for the α-pyrrole carbons is difficult to predict from MO arguments, since both the $3e_g$ and $3a_{2u}$ orbitals have small and roughly equal amounts of spin density on the α-pyrrole carbons, which would cause a decrease and increase in spin density, respectively, as the ruffling is increased according to the model described above. The spin density on the pyrrole nitrogens is also predicted here to increase in the more ruffled variants of *Pa* and *Ht* cytochrome *c*, a result that would also be difficult to predict from MO arguments since both the $3e_g$ and $3a_{2u}$ orbitals have significant electron density on the pyrrole nitrogens. However, ESEEM (or HYSCORE) studies show a *decrease* in the hyperfine couplings of the pyrrole nitrogens upon an increase in ruffling, indicating that a different interpretation is needed.[19] Indeed, DFT models show a complex spin density on the pyrrole nitrogens with an excess of negative spin density;[69] these calculations are consistent with pulsed EPR studies of low-spin ferric porphyrins that indicate negative spin density on the nitrogens.[70−72] Thus, the simple model applied here cannot provide a reliable prediction of spin densities on the pyrrole nitrogens and how they respond to changes in ruffling.

Contributions to the Hyperfine Shifts of Heme Nuclei.

Heme Methyls. The relationships between ruffling and ^{1}H and ^{13}C NMR shift trends for both *Pa* F7A and the *Ht* series of variants are consistent with previous work by Liptak et al.[5] (Tables 1 and 2). The methyl carbons attached to the β-pyrroles are outside of the porphryin π-system, and the ligand-centered pseudocontact shift is expected to be small.[33] However, the amount of ligand-centered pseudocontact shift should be proportional to and have the same sign as the spin density at the β-pyrrole carbons, making it extremely difficult to separate these contributions. Spin polarization occurs as a result of the large spin density on the β-pyrrole carbon that results from the overlap between the d_π (d_{xz}, d_{yz}) orbitals and the porphyrin $3e_g$ orbital. Therefore, the hyperfine shifts of the ^{13}C methyl resonances are negative. The heme ^{1}H methyls are removed from the porphyrin by a second nucleus and therefore are deshielded via a spin polarization mechanism.[37] With increased ruffling, the spin density on the β-pyrrole carbons decreases, and as a result, the average ^{13}C methyl chemical shift increases and the average ^{1}H methyl shift decreases. This pattern is observed in both *Pa* F7A and the *Ht* variants (Tables 1 and 2). In both the *Pa* and *Ht* variants, the change in the metal-centered pseudocontact shift has only a small effect, slightly exaggerating the increase in chemical shift of the ^{13}C methyls and slightly moderating the decrease in chemical shift of the ^{1}H methyls upon an increase in ruffling (Tables 3, S5, and S6).

Heme Mesos. In *Pa* WT, the ^{13}C mesos are shielded relative to the diamagnetic region as a result of spin polarization[5,39] and become slightly less shielded in the more ruffled *Pa* F7A. This same trend in the meso ^{13}C chemical shift is seen in the *Ht* series of variants, which are more ruffled relative to *Ht* WT. This may be attributed to an increase in the d_{xy} character of the SOMO, as shown previously.[5,34] Increased d_{xy} character would increase the distribution of spin density in the porphryin a_{2u} orbital, which has electron density primarily on the pyrrole nitrogens and meso carbons.[68] However, the results show that an increase in spin density on the meso carbons is only partially responsible for the chemical shift changes (Tables 7 and S8−S10). The increase in the meso ^{13}C shift as a result of increased meso carbon spin density is offset by spin polarization from the neighboring α-pyrrole carbons, which have increased spin density with increased ruffling. The two opposing influences are similar in magnitude (Tables 7 and S8−S10), and the overall increased ^{13}C meso shift in the more ruffled variants of *Pa* and *Ht* cytochromes *c* is observed only as a result of a decrease in the contribution of the metal-centered pseudocontact shift (Tables 3, S5, and S6).

The ^{1}H meso shift is likewise determined by competing influences that are similar in magnitude, as previously noted.[29] In *Pa* F7A, the pseudocontact shift for the meso positions becomes less negative as a result of increased ruffling, moving the average ^{1}H meso shift to higher frequency. However, the increase in meso carbon Fermi contact spin density on the more ruffled *Pa* F7A causes a more shielded contact shift. The two competing influences are similar in magnitude (Table 7), explaining why the ^{1}H meso shifts do not move predictably with changes in ruffling. Indeed, in both the *Ht* A7F and *Pa* F7A variants, the average ^{1}H meso shift is more shielded relative to the WT, despite the fact that *Ht* A7F decreases and *Pa* F7A increases heme ruffling. In the *Ht* series of variants as well as the *Pa* F7A variant, a decrease in the average ^{1}H meso shift (Tables 1 and 2) demonstrates that as the ruffling changes, the change in contact shift tends to slightly dominate relative to the change in pseudocontact shift for these systems.

Core Heme Carbons. In *Pa* F7A, a small change of −0.1 ppm relative to *Pa* WT is observed in the average α-pyrrole shift. Across the *Ht* series, a large decrease in α-pyrrole shift (−12 ppm) is observed with an increase in ruffling. Moreover, these shift changes occur in the opposite direction, as predicted by DFT and measured in *Ht* A7F.[5] Therefore, the α-pyrrole ^{13}C shifts do not seem to change predictably with ruffling, indicating complexity in the effect of ruffling on the α-pyrrole ^{13}C shifts, as noted above, and the likelihood that other factors contribute.

This complexity is reflected in the determination of the hyperfine shift components for *Pa* F7A relative to *Pa* WT (Table 7) and for the *Ht* series of variants relative to *Ht* WT (Tables S8−S10). An increase in the α-pyrrole ^{13}C shift in the *Pa* F7A variant results from increased spin density on the α-pyrrole carbon, a decrease in spin density on the neighboring β-pyrrole carbon, and a change in the $\delta_{\mathrm{PC}}^{\mathrm{MC}}$ component (Tables 3, 7, and S5−S10; Figures 6 and 7). However, the spin densities on both the neighboring meso carbon and pyrrole nitrogen increase in the more ruffled cytochrome variants. Both spin density changes contribute to a decreased α-pyrrole ^{13}C shift. The magnitudes of all of the chemical shift components are such that small changes in the relative magnitudes of the various components could affect the direction and magnitude of how ruffling influences the α-pyrrole ^{13}C shift. This is our proposed basis for the discrepancies between the chemical shift changes observed with ruffling for *Ht* A7F, *Pa* F7A, and the *Ht* series studied in this work. The observed decrease in the average β-pyrrole ^{13}C shifts with increased ruffling was expected on the basis of the decrease in spin delocalization of the porphyrin 3e$_g$ orbitals. However, the larger contribution to the decrease in chemical shift was found to be the increased α-pyrrole carbon spin density (Tables 7 and S8−S10). The spin density pattern and how the spin density responds to heme ruffling are illustrated in Figure 9.

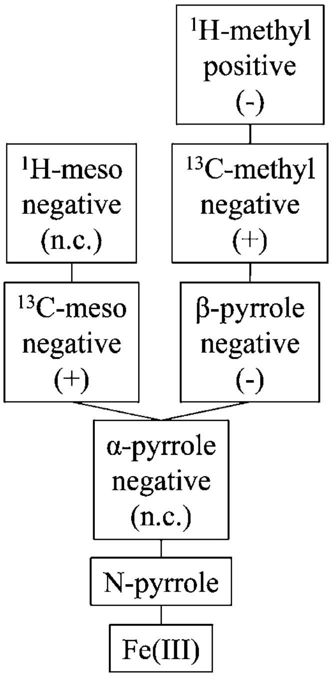

Figure 9. Spin density pattern and connectivity of heme nuclei. "Positive" and "negative" indicate the sign of the hyperfine shifts determined from this work, and (+) and (−) indicate an increase (to higher frequency) and a decrease (to lower frequency) in shifts induced by ruffling, respectively. "n.c." means not consistent; different directions of change of these shifts with increased heme ruffling were observed in different proteins in this study.

Comparison of the *Ht* and *Pa* Variants. The measurement of heme chemical shifts for variants of two different cytochromes *c* increases confidence in the generalizability of these results. Indeed, the delocalized spin densities on the porphyrin ligand nuclei for *Pa* WT and *Ht* WT are similar (Tables 4 and 5). It is possible that the chemical shift changes interpreted in this work are influenced by subtle changes in protein environment or axial ligand interactions rather than by ruffling. However, the same chemical shift trends as a function of ruffling are observed in both the *Pa* F7A variant and the *Ht* series of variants for most nuclei measured. Therefore, it is more likely that ruffling is indeed the major factor influencing the observed heme chemical shift changes. However, there exists some discrepancy in the magnitudes of the chemical shift changes between the *Ht* series and *Pa* F7A. The α- and β-pyrrole ^{13}C shift changes associated with the *Ht* series of mutants herein are much larger than for the *Pa* F7A mutation. It is unlikely that this is explained only by a larger increase in ruffling along the *Ht* series of variants than for *Pa* F7A, since if the chemical shift change were proportional to the change in ruffling, the *Ht* M13V/K22M variant would have to be far more ruffled than any cytochrome *c* previously observed. The larger chemical shift changes seen for the *Ht* series are caused by larger increases in the pyrrole nitrogen, α-pyrrole carbon, and meso carbon spin densities with ruffling. Since the signs of the chemical shift changes are the same for *Pa* F7A and the *Ht* series, the spin densities can be expected to change in the same direction. The origin of the different magnitudes of the spin density changes is not known, but the difference reveals that heme chemical shift changes may not correlate quantitatively to changes in heme ruffling across different species of proteins, although the directions of the changes are expected to be predictive of changes in ruffling. Interestingly, changes in the average ^{1}H methyl shift do not perfectly correlate with changes in the average ^{13}C methyl shift, specifically in the comparison of *Ht* K22M with *Ht* WT and of *Ht* M13V with *Ht* M13V/K22M (Table 2). The heme meso ^{13}C shifts follow the same trend as the heme ^{13}C methyl shift. However, when NMR data from the *Pa* WT, *Pa* F7A, the *Ht* series of variants, and *Ht* A7F[5] are all analyzed, the average ^{1}H heme methyl shift seems to be the best measure of ruffling, providing a consistent general correlation with ruffling in magnitude and direction for all of the variants studied.

Robustness of the Results. The value for *D*, the proportionality constant between the spin density and the ligand-centered pseudocontact shift (eq 11), was calculated herein to be −2872 ppm per electron spin for *Pa* WT and −1279 ppm per electron spin for *Ht* WT. The literature value for an $S = {}^{1}/_{2}$ Fe^{III} porphyrin in the same electron configuration is −6567 ppm per electron spin.[39] A meso-substituted porphyrin was used in the literature determination, contrasting with a β-substituted porphyrin used in this work. This difference in porphryin structure may account for the discrepancy in the literature *D* value from Goff and those from this work. However, there still exists a large difference between the calculated *D* values of the *Pa* and *Ht* proteins. The difference in the *D* value determined could be a result of approximations made in this study. The hemes in this study, because of the substituents and the protein environments, are not fourfold-symmetric, yielding different chemical shifts for each nucleus. For the meso protons, meso carbons, and α-pyrrole carbons, the nuclei are related by a fourfold symmetry axis, so the average $\delta_{\mathrm{con}} + \delta_{\mathrm{PC}}^{\mathrm{LC}}$ term is expected to accurately determine the average spin density. However, the heme methyl carbons are distributed asymmetrically around the heme. Therefore, using the four methyl substituents to calculate the average spin density on all eight β-pyrrole carbons introduces some error. Second, an approximation was necessary to calculate the average β-pyrrole ^{13}C shift: only four of the eight β-pyrrole ^{13}C shifts were measured, and the average $\delta_{\mathrm{obs}} - \delta_{\mathrm{dia}} - \delta_{\mathrm{PC}}^{\mathrm{MC}}$ for these four β-pyrrole carbons was used to approximate the average $\delta_{\mathrm{FC}} + \delta_{\mathrm{PC}}^{\mathrm{LC}}$ of all eight β-pyrrole shifts used for the spin density calculations. This approximation was made because measurement of the other four β-pyrrole shifts would require a different labeling scheme and therefore a different synthesis of ALA. Nevertheless, the large difference between the values of *D* determined here for the two proteins and in previous work by Goff suggests that there are as-yet unknown factors that influence the hyperfine shift.

For the analysis, the calculated value of D was found to be sensitive to changes in the magnitude of the ^{13}C methyl and ^{13}C β shifts, which may account for some of the difference between the calculated and literature values. However, the overall calculated spin densities were not significantly affected, since the spin densities are related primarily to the signs and relative magnitudes of all five nuclear shifts, including the ^{1}H meso, ^{13}C meso, ^{13}C methyl, ^{13}C α-pyrrole and ^{13}C β-pyrrole. The calculated spin densities are not sensitive to changes in the shifts of any one nucleus in particular.

Effect of Ruffling on Pseudocontact Shifts. A change in heme ruffling may alter pseudocontact shifts by changing the positions of nuclei within the paramagnetic anisotropy tensor or by changing the magnetic anisotropy. To determine whether the change in heme structure is sufficient to significantly alter the pseudocontact shifts of peripheral heme nuclei, the crystal structures reported for *Pa* WT (PDB entry 351C)[42] and *Pa* F7A (PDB entry 2EXV)[43] were used for calculations of pseudocontact shifts for the nuclei analyzed in this study. The shifts were calculated for each protein using both structures, and the resulting changes in the spin density differences between *Pa* F7A and *Pa* WT were reevaluated. It was found that the pseudocontact shifts are not significantly affected by the change in heme structure observed between the crystal structures of *Pa* WT and *Pa* F7A, assuming that the magnetic axes and anisotropies remained unaltered.

The orientation of the magnetic axes is not expected to change significantly with ruffling, since this is determined primarily by the orientation of the axial ligands,[29] which are the same in the two crystal structures. However, the values for $\Delta\chi_{ax}$ and $\Delta\chi_{rh}$ can be expected to differ on the basis of the differences in g values measured by EPR (e.g., 3.20, 2.06, and 1.23 for *Pa* WT; 3.15, 2.09, and 1.15 for *Pa* F7A).[34] The differences in $\Delta\chi_{ax}$ and $\Delta\chi_{rh}$ can be estimated from the g values to provide the best estimate of the effect of the *Pa* F7A mutation on the metal-centered pseudocontact shift. The magnetic anisotropy terms cannot be calculated directly from the g values because of a large second-order Zeeman correction.[74] However, since the values of $\Delta\chi_{ax}$ and $\Delta\chi_{rh}$ are known for *Pa* WT, and the g values are known for both *Pa* WT and *Pa* F7A, a simple scaling can be performed to estimate $\Delta\chi_{ax}$ and $\Delta\chi_{rh}$ for *Pa* F7A from the g values. The scaling assumes that the second-order Zeeman correction is proportional to the first-order Zeeman term, which has been calculated from the g values according to the literature.[29] This same estimation of the metal-centered pseudocontact shifts was performed for the *Ht* variants studied in this work using the EPR g values from the literature,[34] and the resulting estimated anisotropy terms are shown in Table S1. The resulting estimated metal-centered pseudocontact shifts assuming no change in magnetic axes are compared for *Pa* F7A and *Pa* WT in Table 3 and for the *Ht* variants relative to *Ht* WT in Tables S5 and S6. The results show that ruffling has a small effect on the pseudocontact shifts of the heme nuclei relative to the changes in contact and ligand-centered pseudocontact shifts. The changes observed are consistent with an increase in rhombicity in the more ruffled variants.

Ruffling and Axial Ligand Bonding. The axial His chemical shifts have previously been measured and analyzed for the *Ht* series.[45,58] The chemical shifts demonstrate an overall increase in the anionic, or histidinate, character of His16 along the *Ht* series. This histidinate character is correlated with an increased His16–Fe^{III} bond strength, as revealed by published work.[58] In particular, the His16 β-^{13}C shift (Figure 4) of the oxidized protein correlates well with the redox potential and is plotted versus the EPR axial terms in Figure 5a, showing a clear trend where the more ruffled variants have a decreased His16 β-^{13}C shift. Furthermore, as the His16–Fe^{III} interaction strengthens and the histidinate character increases, the chemical shifts of the His16 δ-^{15}N and δ-^{1}H nuclei decrease as predicted.[45,75] This observed correlation between ruffling, axial ligand shifts, and heme redox potential provides support for the hypothesis that a change in ruffling modulates the redox potential and may also influence the axial ligand interactions with the heme iron. For the variants studied here, an increase in ruffling correlates with an increase in the His16–Fe^{III} axial ligand bond strength. For heme proteins that bind exogenous ligands, this may be a part of the mechanism by which ligand binding properties can be modulated by the protein.[19] As the axial His becomes a better donor, the iron Z_{eff} decreases, increasing the energies of the Fe orbitals and influencing the binding to ligands.[76]

The mutations made in this work are on the proximal side of the heme, suggesting that the changes to the axial Met61 ε-C^{1}H$_3$ hyperfine shift are indirect as a result of the changes in heme conformation or a result of a change in the His16–Fe^{III} interaction. The analysis of the δ_{PC}^{MC} values for both *Pa* WT and *Pa* F7A demonstrates that the axial Met hyperfine shift change with ruffling is primarily a result of the Fermi contact contribution. Among the proteins studied here, the Fermi contact contribution to the axial Met61 ε-C^{1}H$_3$ shift increases with increased ruffling, which is the opposite trend as predicted by an earlier DFT analysis.[5] A weakening of the Met61–Fe^{III} bond is expected when considering the trans effect with a stronger His16–Fe^{III} interaction occurring across the series,[58] which would decrease the Fermi contact shift on Met61. The basis for the observed trend is not currently understood.

It has been proposed that the redox potential is lowered by increased heme ruffling.[5,9,10] This correlation is observed for the variants studied in this work. *Pa* F7A, *Ht* K22M, *Ht* M13V, and *Ht* M13V/K22M have previously been determined to have lower redox potentials relative to their respective WT proteins, and among the *Ht* series of mutants, the potential decreases as ruffling increases.[45,77] The results here support a general trend between increased ruffling and decreased redox potential.

■ CONCLUSIONS

Heme chemical shifts of variants of two different bacterial cytochromes *c* demonstrate that ruffling influences low-spin Fe(III) heme hyperfine NMR shifts in a way that is predictable and well-understood for most heme nuclei. An analysis of the metal-centered pseudocontact, ligand-centered pseudocontact, and Fermi contact shifts shows how ruffling influences each of these components for heme nuclei. The paramagnetic shifts were analyzed to evaluate delocalized spin densities on the porphyrin ring, demonstrating that an increase in ruffling decreases the spin density on the β-pyrrole carbons while increasing the spin densities on the meso carbons and α-pyrrole carbons. In addition, heme ruffling correlates with the axial histidine chemical shifts, with an increase in ruffling correlating with an increase in the axial His–Fe^{III} bond strength. This provides further evidence that heme ruffling may influence axial ligand bonding properties that are important for the function of many heme proteins.

■ ASSOCIATED CONTENT

Ⓢ Supporting Information

NMR spectra (14 figures), data plots (2 figures), two equations, and 14 tables, including complete lists of individual chemical shifts used. This material is available free of charge via the Internet at http://pubs.acs.org.

■ AUTHOR INFORMATION

Corresponding Author

*E-mail: bren@chem.rochester.edu.

Notes

The authors declare no competing financial interest.

■ ACKNOWLEDGMENTS

The authors acknowledge funding from NIH (GM63170) and thank Linda Thöny-Meyer for the gift of pEC86.

■ REFERENCES

(1) Shelnutt, J. A.; Song, X. Z.; Ma, J. G.; Jia, S. L.; Jentzen, W.; Medforth, C. J. *Chem. Soc. Rev.* **1998**, *27*, 31−41.

(2) Jentzen, W.; Song, X. Z.; Shelnutt, J. A. *J. Phys. Chem. B* **1997**, *101*, 1684−1699.

(3) Jentzen, W.; Ma, J. G.; Shelnutt, J. A. *Biophys. J.* **1998**, *74*, 753−763.

(4) Howes, B. D.; Brissett, N. C.; Doyle, W. A.; Smith, A. T.; Smulevich, G. *FEBS J.* **2005**, *272*, 5514−5521.

(5) Liptak, M. D.; Wen, X.; Bren, K. L. *J. Am. Chem. Soc.* **2010**, *132*, 9753−9763.

(6) Hagarman, A.; Duitch, L.; Schweitzer-Stenner, R. *Biochemistry* **2008**, *47*, 9667−9677.

(7) Gruia, F.; Kubo, M.; Ye, X.; Ionascu, D.; Lu, C.; Poole, R. K.; Yeh, S. R.; Champion, P. M. *J. Am. Chem. Soc.* **2008**, *130*, 5231−5244.

(8) Bowman, S. E. J.; Bren, K. L. *Nat. Prod. Rep.* **2008**, *25*, 1118−1130.

(9) Shokhireva, T. K.; Berry, R. E.; Uno, E.; Balfour, C. A.; Zhang, H. J.; Walker, F. A. *Proc. Natl. Acad. Sci. U.S.A.* **2003**, *100*, 3778−3783.

(10) Roberts, S. A.; Weichsel, A.; Qiu, Y.; Shelnutt, J. A.; Walker, F. A.; Montfort, W. R. *Biochemistry* **2001**, *40*, 11327−11337.

(11) Olea, C.; Boon, E. M.; Pellicena, P.; Kuriyan, J.; Marletta, M. A. *ACS Chem. Biol.* **2008**, *3*, 703−710.

(12) Maes, E. M.; Roberts, S. A.; Weichsel, A.; Montfort, W. R. *Biochemistry* **2005**, *44*, 12690−12699.

(13) Fernandez, M. L.; Estrin, D. A.; Bari, S. E. *J. Inorg. Biochem.* **2008**, *102*, 1523−1530.

(14) Caignan, G. A.; Deshmukh, R.; Zeng, Y. H.; Wilks, A.; Bunce, R. A.; Rivera, M. *J. Am. Chem. Soc.* **2003**, *125*, 11842−11852.

(15) Ukpabi, G.; Takayama, S.-i. J.; Mauk, A. G.; Murphy, M. E. P. *J. Biol. Chem.* **2012**, *287*, 34179−34188.

(16) Nambu, S.; Matsui, T.; Goulding, C. W.; Takahashi, S.; Ikeda-Saito, M. *J. Biol. Chem.* **2013**, *288*, 10101−10109.

(17) Matsui, T.; Nambu, S.; Ono, Y.; Goulding, C. W.; Tsurnoto, K.; Ikeda-Saito, M. *Biochemistry* **2013**, *52*, 3025−3027.

(18) Singh, R.; Berry, R. E.; Yang, F.; Zhang, H. J.; Walker, F. A.; Ivancich, A. *Biochemistry* **2010**, *49*, 8857−8872.

(19) Van Doorslaer, S.; Tilleman, L.; Verrept, B.; Desmet, F.; Maurelli, S.; Trandafir, F.; Moens, L.; Dewilde, S. *Inorg. Chem.* **2012**, *51*, 8834−8841.

(20) Lu, H.; Zhang, X. P. *Chem. Soc. Rev.* **2011**, *40*, 1899−1909.

(21) Honda, T.; Kojima, T.; Fukuzumi, S. *J. Am. Chem. Soc.* **2012**, *134*, 4196−4206.

(22) Caselli, A.; Gallo, E.; Ragaini, F.; Ricatto, F.; Abbiati, G.; Cenini, S. *Inorg. Chim. Acta* **2006**, *359*, 2924−2932.

(23) Gazeau, S.; Pecaut, J.; Haddad, R.; Shelnutt, J. A.; Marchon, J. C. *Eur. J. Inorg. Chem.* **2002**, 2956−2960.

(24) Grinstaff, M. W.; Hill, M. G.; Birnbaum, E. R.; Schaefer, W. P.; Labinger, J. A.; Gray, H. B. *Inorg. Chem.* **1995**, *34*, 4896−4902.

(25) Li, X. Y.; Czernuszewicz, R. S.; Kincaid, J. R.; Spiro, T. G. *J. Am. Chem. Soc.* **1989**, *111*, 7012−7023.

(26) Schweitzer-Stenner, R. *J. Porphyrins Phthalocyanines* **2001**, *5*, 198−224.

(27) Zhu, L. Y.; Zhong, G.; Unno, M.; Sligar, S. G.; Champion, P. M. *Biospectroscopy* **1996**, *2*, 301−309.

(28) Shokhireva, T. K.; Weichsel, A.; Smith, K. M.; Berry, R. E.; Shokhirev, N. V.; Balfour, C. A.; Zhang, H.; Montfort, W. R.; Walker, F. A. *Inorg. Chem.* **2007**, *46*, 2041−2056.

(29) Shokhirev, N. V.; Walker, F. A. *J. Biol. Inorg. Chem.* **1998**, *3*, 581−594.

(30) Shokhireva, T. K.; Shokhirev, N. V.; Walker, F. A. *Biochemistry* **2003**, *42*, 679−693.

(31) Walker, F. A. *J. Biol. Inorg. Chem.* **2006**, *11*, 391−397.

(32) Zhong, L.; Wen, X.; Rabinowitz, T. M.; Russell, B. S.; Karan, E. F.; Bren, K. L. *Proc. Natl. Acad. Sci. U.S.A.* **2004**, *101*, 8637−8642.

(33) Banci, L.; Bertini, I.; Luchinat, C.; Pierattelli, R.; Shokhirev, N. V.; Walker, F. A. *J. Am. Chem. Soc.* **1998**, *120*, 8472−8479.

(34) Can, M.; Zoppellaro, G.; Andersson, K. K.; Bren, K. L. *Inorg. Chem.* **2011**, *50*, 12018−12024.

(35) Shokhireva, T. K.; Shokhirev, N. V.; Berry, R. E.; Zhang, H. J.; Walker, F. A. *J. Biol. Inorg. Chem.* **2008**, *13*, 941−959.

(36) Zoppellaro, G.; Harbitz, E.; Kaur, R.; Ensign, A. A.; Bren, K. L.; Andersson, K. K. *J. Am. Chem. Soc.* **2008**, *130*, 15348−15360.

(37) Walker, F. A. *Inorg. Chem.* **2003**, *42*, 4526−4544.

(38) Rivera, M.; Caignan, G. A. *Anal. Bioanal. Chem.* **2004**, *378*, 1464−1483.

(39) Goff, H. M. *J. Am. Chem. Soc.* **1981**, *103*, 3714−3722.

(40) Wang, W.; Ye, X.; Demidov, A. A.; Rosca, F.; Sjodin, T.; Cao, W. X.; Sheeran, M.; Champion, P. M. *J. Phys. Chem. B* **2000**, *104*, 10789−10801.

(41) Hobbs, J. D.; Shelnutt, J. A. *J. Protein Chem.* **1995**, *14*, 19−25.

(42) Matsuura, Y.; Takano, T.; Dickerson, R. E. *J. Mol. Biol.* **1982**, *156*, 389−409.

(43) Borgia, A.; Bonivento, D.; Travaglini-Allocatelli, C.; Di Matteo, A.; Brunori, M. *J. Biol. Chem.* **2006**, *281*, 9331−9336.

(44) Karan, E. F.; Russell, B. S.; Bren, K. L. *J. Biol. Inorg. Chem.* **2002**, *7*, 260−272.

(45) Michel, L. V.; Ye, T.; Bowman, S. E. J.; Levin, B. D.; Hahn, M. A.; Russell, B. S.; Elliott, S. J.; Bren, K. L. *Biochemistry* **2007**, *46*, 11753−11760.

(46) Russell, B. S.; Zhong, L.; Bigotti, M. G.; Cutruzzolà, F.; Bren, K. L. *J. Biol. Inorg. Chem.* **2003**, *8*, 156−166.

(47) Arslan, E.; Schulz, H.; Zufferey, R.; Kunzler, P.; Thöny-Meyer, L. *Biochem. Biophys. Res. Commun.* **1998**, *251*, 744−747.

(48) Rivera, M.; Walker, F. A. *Anal. Biochem.* **1995**, *230*, 295−302.

(49) Wang, J. J.; Scott, A. I. *Tetrahedron Lett.* **1997**, *38*, 739−740.

(50) Horio, T.; Higashi, T.; Sasagawa, M.; Kusai, K.; Nakai, M.; Okunuki, K. *Biochem. J.* **1960**, *77*, 194−201.

(51) Delaglio, F.; Grzesiek, S.; Vuister, G. W.; Zhu, G.; Pfeifer, J.; Bax, A. *J. Biomol. NMR* **1995**, *6*, 277−293.

(52) Chen, V. B.; Arendall, W. B., III; Headd, J. J.; Keedy, D. A.; Immormino, R. M.; Kapral, G. J.; Murray, L. W.; Richardson, J. S.; Richardson, D. C. *Acta Crystallogr., Sect. D: Biol. Crystallogr.* **2010**, *66*, 12−21.

(53) Emerson, S. D.; La Mar, G. N. *Biochemistry* **1990**, *29*, 1556−1566.

(54) Takayama, S. J.; Takahashi, Y.; Mikami, S.; Irie, K.; Kawano, S.; Yamamoto, Y.; Hemmi, H.; Kitahara, R.; Yokoyama, S.; Akasaka, K. *Biochemistry* **2007**, *46*, 9215−9224.

(55) Travaglini-Allocatelli, C.; Gianni, S.; Dubey, V. K.; Borgia, A.; Di Matteo, A.; Bonivento, D.; Cutruzzolà, F.; Bren, K. L.; Brunori, M. *J. Biol. Chem.* **2005**, *280*, 25729−25734.

(56) Timkovich, R.; Cai, M. L.; Zhang, B. L.; Arciero, D. M.; Hooper, A. B. *Eur. J. Biochem.* **1994**, *226*, 159−168.

(57) Timkovich, R. *Inorg. Chem.* **1991**, *30*, 37−42.

(58) Bowman, S. E. J.; Bren, K. L. *Inorg. Chem.* **2010**, *49*, 7890−7897.

(59) Walker, F. A. *Coord. Chem. Rev.* **1999**, *186*, 471−534.

(60) Kurland, R. J.; McGarvey, B. R. *J. Magn. Reson.* **1970**, *2*, 286−301.

(61) Jesson, J. P. In *NMR of Paramagnetic Molecules*; La Mar, G. N., Horrocks, W. D., Jr., Holm, R. H., Eds.; Academic Press: New York, 1973.

(62) Turner, D. L. *Eur. J. Biochem.* **1993**, *211*, 563−568.

(63) Karplus, M.; Fraenkel, G. K. *J. Chem. Phys.* **1961**, *35*, 1312−1323.

(64) Ikeue, T.; Ohgo, Y.; Saitoh, T.; Nakamura, M.; Fujii, H.; Yokoyama, M. *J. Am. Chem. Soc.* **2000**, *122*, 4068−4076.

(65) Niibori, Y.; Ikezaki, A.; Nakamura, M. *Inorg. Chem. Commun.* **2011**, *14*, 1469−1474.

(66) It is important to note that *D* here is not the zero-field splitting, which also is typically denoted as "*D*".

(67) Rivera, M.; Qiu, F.; Bunce, R. A.; Stark, R. E. *J. Biol. Inorg. Chem.* **1999**, *4*, 87−98.

(68) Nakamura, M. *Coord. Chem. Rev.* **2006**, *250*, 2271−2294.

(69) Johansson, M. P.; Sundholm, D.; Gerfen, G.; Wikstrom, M. *J. Am. Chem. Soc.* **2002**, *124*, 11771−11780.

(70) Scholes, C. P.; Falkowski, K. M.; Chen, S.; Bank, J. *J. Am. Chem. Soc.* **1986**, *108*, 1660−1671.

(71) Magliozzo, R. S.; Peisach, J. *Biochemistry* **1992**, *31*, 189−199.

(72) Garcia-Rubio, I.; Mitrikas, G. *J. Biol. Inorg. Chem.* **2010**, *15*, 929−941.

(73) Shokhirev, N. V., 2009; downloaded from www.shokhirev.com.

(74) Horrocks, W. D.; Greenberg, E. S. *Biochim. Biophys. Acta* **1973**, *322*, 38−44.

(75) Banci, L.; Bertini, I.; Turano, P.; Tien, M.; Kirk, T. K. *Proc. Natl. Acad. Sci. U.S.A.* **1991**, *88*, 6956−6960.

(76) Das, P. K.; Chatterjee, S.; Samanta, S.; Dey, A. *Inorg. Chem.* **2012**, *51*, 10704−10714.

(77) Takayama, S. J.; Irie, K.; Tai, H. L.; Kawahara, T.; Hirota, S.; Takabe, T.; Alcaraz, L. A.; Donaire, A.; Yamamoto, Y. *J. Biol. Inorg. Chem.* **2009**, *14*, 821−828.